Investigation of charge carrier dynamics in positive lithium-ion battery electrodes via optical in situ observation

Florian Rittweger[a,*], Christian Modrzynski[a,b], Valentin Roscher[a], Dmitry L. Danilov[c,d], Peter H. L. Notten[c,d,e], Karl-Ragmar Riemschneider[a]

[a] *University of Applied Sciences Hamburg, Berliner Tor 7, DE-20099 Hamburg, Germany*
[b] *University of Waterloo, 200 University Avenue W, Waterloo ON N2L 3G1, Canada*
[c] *Forschungszentrum Jülich (IEK-9), Ostring 10, DE-52425 Jülich, Germany*
[d] *Eindhoven University of Technology, De Zaale, NL-5612 AZ Eindhoven, the Netherlands*
[e] *University of Technology Sydney, Broadway, Sydney, NSW 2007, Australia*

Abstract

We present optical in situ investigations of lithium-ion dynamics in lithium iron phosphate based positive electrodes. The change in reflectivity of these cathodes during charge and discharge is used to estimate apparent diffusion coefficients for the lithiation and delithiation process of the entire electrode. Thereby, a scaling analysis of the transport process is applied, which clearly reveals its diffusive character.

Results are shown for cathodes, in which the common additive carbon as well as the conductive and electrochromic marker additives (indium tin oxide and antimony tin oxide) are used. The latter leads to a substantial increase of visibility of the optical effect in the cathodes while electric properties remain qualitatively unchanged.

The procedure extends common characterization techniques of positive electrode materials via a novel and integral combination of electrical and optical measurements.

Keywords: Lithium-ion battery, Lithium iron phosphate, Material characterization, In situ video microscopy, Transparent conducting oxides, Diffusion coefficient

*Corresponding author; florian.rittweger@haw-hamburg.de; +4940428758425

1. Introduction

The rapidly increasing demand of rechargeable lithium-ion batteries in numerous applications such as portable electronic devices, electric vehicles and energy storage systems with very different performance and safety requirements provides challenging tasks for battery material researchers. Macroscopical properties like energy and power density or long-term cycling stability are ideally based on microscopical observations of structural material changes, dendritic growth and charge carrier dynamics. Especially the latter is important for understanding the electrical behavior of the battery and to model and simulate batteries [1–9] as well as to design future lithium-ion chemistries. There are several standard methods for characterization of the dynamical properties of mass and charge transport in Li-ion batteries. The potentiostatic intermittent titration technique (PITT) involves imposing the step change in the potential across the cell was well described in [10]. The galvanostatic intermittent titration technique (GITT), based on the application of rectangular current pulses, goes back to the seminal works of Wepper [11] and Wen [12], who introduced the method and derived basic formalism. PITT/GITT methods were used during subsequent decades to investigate properties of various materials, such as lithium cobalt oxide (LCO) thin films [13, 14], Nickel-Manganese-Cobalt (NMC) powders [15], lithium-, sodium- and potassium-ion systems [16], aluminum-ion cathodes [17]. Aging experiments [18] and tests for the parametrization of electrochemical models [19] is also a frequent application area. Also, the electrochemical impedance spectrum (EIS) can be used to determine the apparent diffusion coefficient [20, 21]. A fundamental overview of diffusion-related phenomena can be found in [22]. Diffusion limitations normally lead to the formation of concentration profiles inside active electrode material therefore the investigation of such profiles represents considerable scientific interest. The neutron depth profiling (NDP) represents a powerful tool for accessing concentration profiles in various porous [23] and thin-film [24] systems. Recently, optical investigations,

which are more easily accessible, were presented to study dynamics in negative electrodes based on graphite [25–27], while, to the best of our knowledge, a similar quantitative method is missing for positive electrodes.

For this reason, we present a method to calculate *apparent* diffusion coefficients D of lithium iron phosphate (LFP) based cathodes purely from optical measurements within a macroscopical description with Fick's second law. Thereby, our method takes care of the phase changing nature of LFP upon lithiation and delithiation, which is related to a change in reflectivity. The as-obtained D has to be understood as a combination of the microscopic processes of migration and diffusion of lithium ions within the liquid electrolyte and the electrochemical (dis)charge reaction taking place at the surface of the solid LFP particles. Therefore, the obtained diffusion coefficient do not describe the microscopic ion dynamics within a single particle of the active cathode material but it yields comprehensive information about the macroscopic dynamics of the entire electrode with its specific properties including porosity, tortuosity and thickness.

We further report primarily on antimony tin oxide (ATO) nanopowder as an electrode additive to enhance the optical observability of the LFP cathode due to the replacement of the usual carbon (C) nanopowder as conductive agent. Overall, ATO behaves similar to indium tin oxide (ITO), which we used previously [28–30], but offers some advantages as discussed later on. For this reason, the estimation of the apparent diffusion coefficient is discussed in details only for the LFP/ATO cathode in the present manuscript. Results for the LFP/ITO and LFP/C cathode are given in the Supplemental Material. Nevertheless, the step-by-step results are very similar, which indicate that the method can be easily transferred to investigate other positive electrodes as well.

2. Experimental

2.1. Material Preparation

Cathodes were prepared from slurries, which consist of lithium iron phosphate (LFP, Südchemie) and a nanopowder as additive, which is either carbon

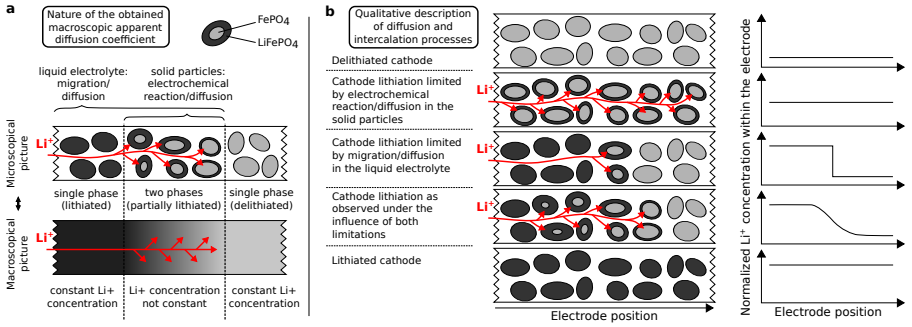

Figure 1: **Microscopical lithiation process and macroscopical observation** (a) Illustration of the microscopic origin of the obtained apparent diffusion coefficient from a macroscopical observation of the LFP cathode. The one-dimensional transportation pathway of lithium ions is sketched with red arrows. Shown are processes affecting the diffusion coefficient and their local appearance in the electrode. Within the central region, the three processes can't be clearly distinguished, which means that the obtained diffusion coefficient is a combination of those processes, i.e. an apparent quantity. (b) Qualitative description of scenarios of cathode lithiation during the intercalation process. Shown are microscopical sketches (center) of the lithiation process under different ion transport limitations (left) and the resulting concentration profile of lithium ions in the macroscopical LFP electrode (right).

(C), indium tin oxide (ITO) or antimony tin oxide (ATO) as well as polyvinylidene difluoride (PVDF) dissolved in N-methylpyrrolidone (NMP) as a binder (all Sigma-Aldrich). According to the producer, ITO and ATO particles are smaller than 50 nm. Using a doctor blade method, the slurries were coated on aluminum foils with a blade height of 200 μm. Afterwards the cathodes were left to dry under an infrared lamp for 30 min and were heated at 100 °C under vacuum for 1 h. For each cathode, the mass fraction of active material, additive and binder is 90% LFP, 5% ATO/ITO/C and 5% PVDF, respectively. The thickness of the resulting electrode foils was measured with a Heidenhain measuring sensor. The averaged thicknesses from several spots at the electrodes are 49.0 μm, 31.5 μm and 41.5 μm with deviations of $\sim$10% for LFP/ATO, LFP/ITO and LFP/C, respectively. The electrode area was $\sim$1.2 cm^2 each. To avoid capacity mismatches between the anode and the cathode leading to insufficient lithiation, we used a plate of lithium metal as counter electrode. Finally, a glass fiber separator (EL-Cell GmbH) and approximately 100 μl 1M lithium hexafluorophosphate ethylene/propylene carbonate electrolyte solution (Sigma-Aldrich) were used for cell assembly in a glovebox.

Upon charging and discharging, the cathode is delithiated and lithiated according to the electrochemical (dis)charge reaction, taking place at the surface of the solid LFP particles:

$$\mathrm{LiFe^{(II)}PO_4} \rightleftharpoons \mathrm{Fe^{(III)}PO_4} + \mathrm{Li^+} + \mathrm{e^-} \quad . \tag{1}$$

On a microscopical scale, LFP is a two-phase material, which undergoes a phase transition upon lithiation and delithiation described by several models [5, 31–36]. We suppose, that this two-phase nature can be transferred to a macroscopical description of the entire electrode by means of lithiated and delithiated cathode regions, i.e. dark and bright regions, with well defined concentrations of lithium ions. Simplified illustrations for this description are shown in figure 1. Also shown are intercalation processes, which are limited by either ion dynamics in the electrolyte or in the solid particles, and the resulting concentration profile of lithium ions over the entire electrode. As seen from the sketched graphs and shown later on in the measurements, the obtained concentration profiles with the intercalation front as boundary region between the lithiated and delithiated region, appear as a combination of both ion dynamics.

2.2. Electrode and Measurement Setup

The electrode stack of the battery was placed in the windowed test cell ECC-Opto-Std (EL-Cell GmbH) in such a way, that the cathode was directly observable from top during battery cycling (figure 2(a)). By construction, lithium ions (red arrow) can enter and leave the LFP cathode only at the separator/cathode edge in x-direction (d). Due to the overlap of the cathode with the cell housing (b), an ionic transport in y-direction is minor and can be neglected. Additionally, the ionic transport in z-direction from the lithium metal into the LFP is blocked by the current collector. Thus, the optical properties of the cathode can be studied in a one-dimensional way.

We used in-house developed hard- and software solutions to monitor the cycling process as well as the voltage and current measurements of the test cell. The initial C rate in the constant current (CC) charging and discharging

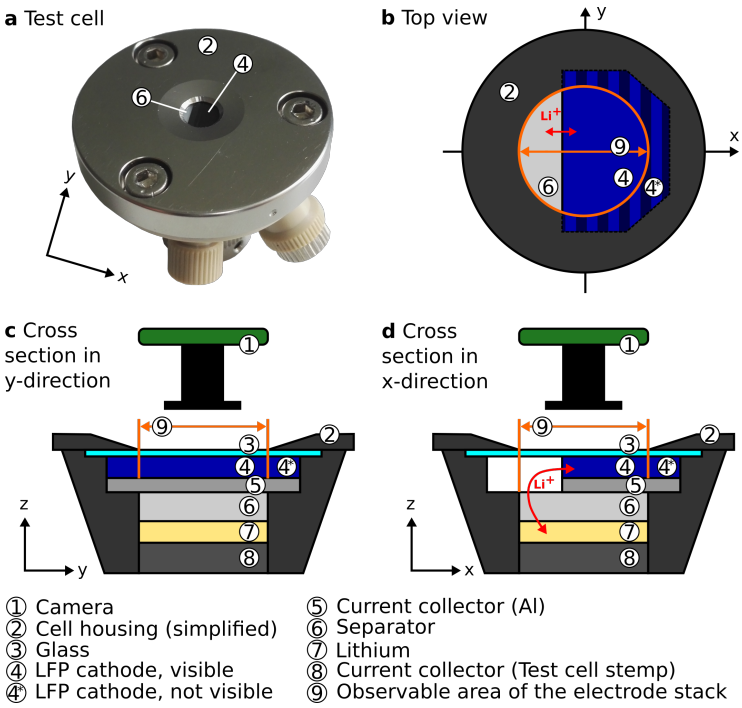

Figure 2: **Experimental setup and electrode arrangement** (a) Optical test cell ECC-Opto-Std (EL-Cell) used for the in situ observation of lithium (de)intercalation in LFP/X cathodes, where X represents the additives ATO, ITO or C. (b)-(d) Top view and cross sections of the test cell showing the structure and geometry of the electrode stack. The pathway of lithium ions is highlighted as red arrow showing that ion (de)intercalation can only take place at the cathode/separator boundary region. Hence, the latter is a one-dimensional process in x-direction.

modes was C/4 or less. However, it reduced significantly below C/10 during the evaluation of the diffusion coefficient in the related constant voltage (CV) modes. Thus, CCCV cycling profiles were applied both for charging and discharging. The electrical charge was calculated via integration over the current known as *coulomb counting*. Upon cycling, voltage limits were set to 2.8 V and 3.8 V for the lower and upper limit, respectively.

The test cell was illuminated with white LEDs, which offer a broad distributed spectrum of wavelengths in the range of 380 nm to 780 nm (Adafruit, NeoPixel Ring). The obtained intensities in the color channels red, green and blue of the camera are referred to as reflected light from the electrodes. To neglect influences from ambient light, the measurement setup including test cell

and camera was placed in a box. The camera setup consists of the *mvBlueFOX-MLC205C* and an S-Mount objective (both MatrixVision), which leads to a spatial resolution of roughly 5 μm/pixel. Images were recorded once every minute, which is sufficient with respect to the chemical processes being macroscopically observed in this setup. Post-processing as well as further calculations and visualizations were performed within the MATLAB software environment.

3. Results and Discussion

3.1. Comparison of electrochromic marker materials and carbon as cathode additive

Up to now, we claimed, that it is necessary to replace the carbon additive by an electrochromic marker additive (ITO or ATO) to enable an optical observation of the - usually black - cathode. As seen in figure 3(c1), this holds for moderate exposure times during image recording. Increasing the sensitivity of the camera and the exposure time significantly (figures 3(c1)-(c3) and 3(c)), we were also able to observe a change in the reflectivity during charge and discharge cycles for an LFP cathode, built with the common conductive agent carbon. Thereby, the sensitivity of the camera was enhanced due to a doubled dB-Gain offset and the exposure time was doubled during image recording. Nevertheless, using the electrochromic markers ITO and ATO, the reflectivity differences and hence the varying concentration of lithium ions within the LFP cathode can be measured more easily and is clearly visible without specific camera settings (figures 3(a) and (b)).

Regarding the selection of electrochromic markers, ATO has some major advantages compared to ITO. First, it is cheaper than ITO by roughly a factor of 10. Second, its mixing behavior with other slurry components is much more favorable with respect to mixing time, effort and stability. Furthermore, its related optical and electrical properties within the battery electrode are almost the same as for ITO.

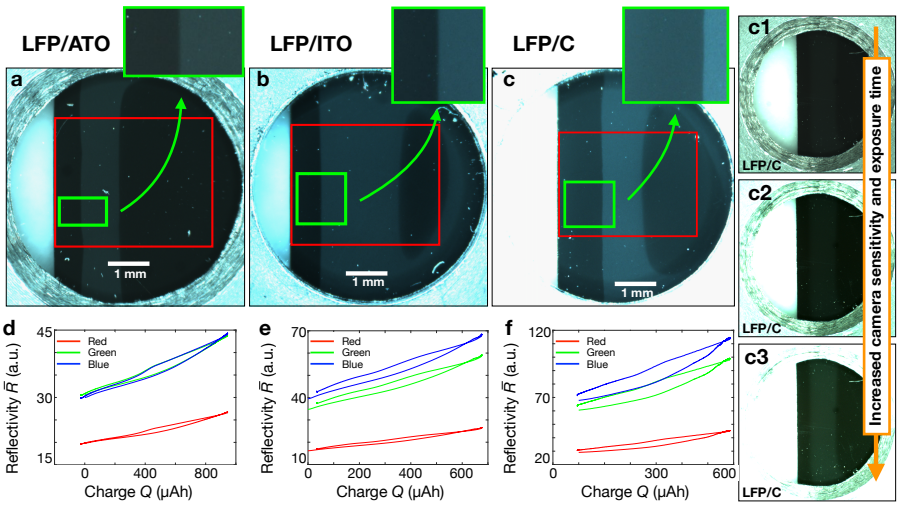

Figure 3: **Camera images of the LFP cathodes** (a)-(c) Camera images of the LFP/ATO, LFP/ITO and LFP/C cathodes (dark areas) taken at the constant voltage mode at 2.8 V and electrical charges $Q \approx \{307, 156, 113\}$ μAh while discharging the battery. Thereby, Q is calculated from the whole electrode. (d)-(f) Reflectivity-charge correlation, $\overline{R}(Q)$ for a whole charge and discharge cycle, with $\overline{R}$ being obtained only from a visible part of the cathode (red rectangles). The highlighted cathode areas in green rectangles are investigated in details to estimate apparent diffusion coefficients. Bright and dark areas refer to regions in the cathode, which are delithiated or lithiated, respectively. Due to construction, the intercalation and deintercalation of lithium ions into the cathode is solely possible at the separator/cathode boundary at the left hand side. (c1)-(c3) Another LFP/C cathode at the same lithiated state but with different camera recording setups.

3.2. Correlation of reflectivity and electrical charge

The total reflectivity of the cathode $\overline{R}$ is calculated as normalized average from the spatially resolved reflectivity R at each image pixel, $\overline{R} = \langle R(x, y) \rangle_{x,y}$. A comparison with the electrical charge Q reveals that bright cathode areas correspond to a charged battery state, i.e. a delithiated cathode, and dark cathode areas correspond to a discharged battery state, i.e. a lithiated cathode [29]. Figure 3 depicts this observation for all three cathodes. Nevertheless, a complete correlation between $\overline{R}$ and Q can not be given since the cathodes are only partially observable (see figure 2(b)) while Q is obtained from the entire cathode. For the dependencies $\overline{R}(Q)$, which are shown in figures 3(d)-(f), only the areas within the red rectangles figures 3(a)-(c) are evaluated for $\overline{R}$.

As seen in figures 3(d)-(f) the three color channels of the camera (red, green

and blue) varying similarly during cycling for all three cathode materials. Hence, only a change in brightness is observed. Further calculations are therefore based on the intensity values of the green color channel of the camera, which is referred to as reflectivity from here on.

3.3. From reflectivity to lithium concentration

Figure 4(a) shows the current and voltage profiles for a charge/discharge cycle. During charging, the constant current leads to a voltage increase until the whole separator/cathode boundary region is fully delithiated. Subsequently, the potential is held at 3.8 V for at least 20 h leading to a decreasing current. Afterwards an open circuit rest period is applied for 2 h. Figures 4(b) and (c) show images of the evaluated cathode region upon charge (i)-(iv) and discharge (v)-(viii). Thereby, the images correspond to the highlighted green rectangles in figure 3(a). Lithiated and delithiated areas are clearly seen as dark and bright areas and the sharp boundary region, which separates both areas is identified as intercalation or deintercalation front depending on the moving direction of the lithium ions. Taking a closer look at 4(b), one can see, that the deintercalation front is almost straight and moves from left to right with time, which means that it moves from the separator/electrode interface towards the bulk of the electrode. The same observation holds for the discharge process, with lithiation starting at the separator/electrode interface (v)-(viii). Hence, the chosen measurement setup, shown in figure 2, enables an investigation of the optical properties in a one-dimensional way.

The reflectivity obtained from the highlighted green area in figure 3(a) is shown in figure 5 for charge (a) and discharge (b). The two-dimensional spatial reflectivity $R(x, y)$ is averaged in y-direction leading to the shown one-dimensional quantity $R(x) = \langle R(x, y) \rangle_y$. The latter can be related to the concentration of lithium ions as described below. Each line in figures 5(a) and (b) corresponds to a measured reflectivity taken in one hour time steps. In the beginning of the experiment, the evaluated cathode region was fully lithiated. Hence, R is low at the start of the charge process (lower blue curve, S_c) through-

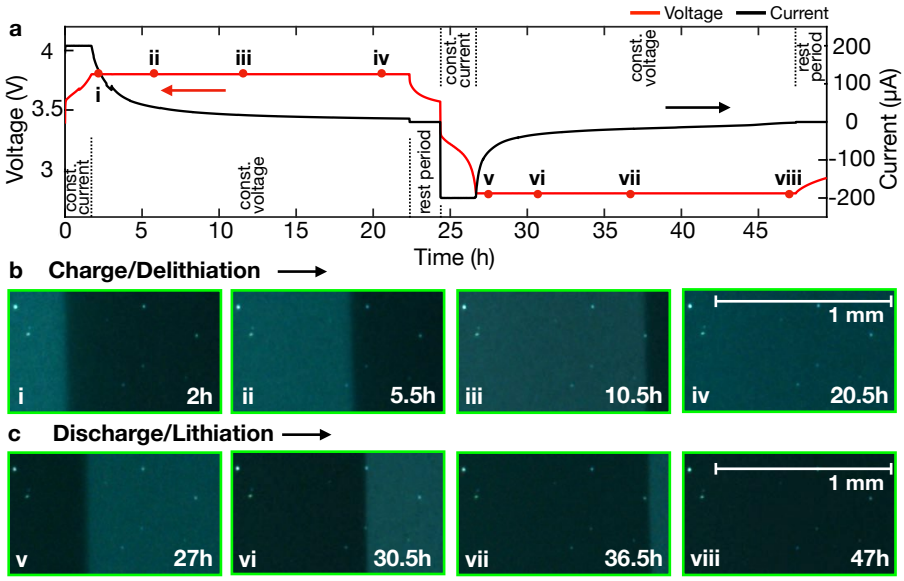

Figure 4: **Electrical data and optical observation of the evaluated area** (a) Voltage and current profile of a charge/discharge cycle for the Li-LFP/ATO battery. (b) and (c) Images of the selected cathode region, which is highlighted with a green rectangle in figure 3(a), at different times during the experiment during charge and discharge. The intercalation front is clearly visible separating lithiated (dark) and delithiated (bright) regions in the cathode.

out x, which is the position at the electrode. While the battery is charged and the cathode is delithiated, R increases with time from left to right until the evaluated region is fully delithiated (turquoise blue, E_c). After a two hour rest period (P, green), the battery is discharged leading to the complementary result (b). The sharp decrease of R along x marks the deintercalation and intercalation front, which is visible in the camera images in figures 3 and 4 as separation of bright and dark cathode areas.

The evaluation of apparent diffusion coefficients from the (de)intercalation front requires the formulation of a bijective relation between the reflectivity R and the lithium concentration c in the cathode. As a first step, the reflectivity was normalized to the interval [0,1] for a lithiated and delithiated cathode, respectively, using the baseline fits shown in figure 5. Afterwards, this normalized reflectivity $\widetilde{R}$ was used to calculate the lithium concentration as

$$c = c_{\max} \times (1 - \widetilde{R}) \quad , \tag{2}$$

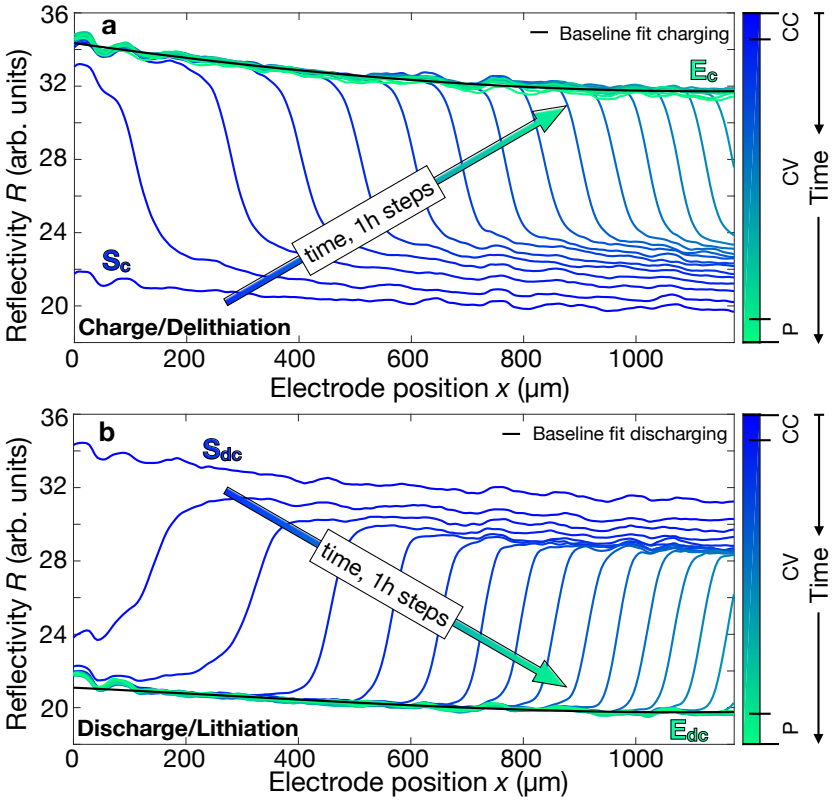

Figure 5: **Reflectivity profiles** Estimated reflectivity of the LFP/ATO cathode (green rectangle in figure 3(a)) perpendicular to the lithium intercalation front while charging (a) and discharging (b). The color code marks the experimental time and the cycling modes (CC, CV and P), which are shown in details in figure 4. Lines are drawn in one hour steps. Additionally, the lines marked with S_c, E_c, S_{dc} and E_{dc} highlight the begin of the CC mode (S) and the end of the CV mode (E) in both charge and discharge processes. Larger values of the reflectivity are related to a brighter and more delithiated cathode. The same holds vice versa for lower reflectivities. The black lines refer to baseline fits at the end of each constant voltage mode.

with $c_{\max}$ being the maximal concentration of lithium within LFP. The result of this transformation is shown in figure 6.

Interestingly, figure 6 shows, that (de)lithiation of the cathode does not only take place within a small region around the (de)intercalation front as one might expect. For instance, looking at $x \approx 1000\,\mu$m in figure 6(a), the lithium concentration decreases already in the constant current mode despite the fact, that the deintercalation front is still far away (compare upper yellow and lower magenta curve). As soon as the charge process starts, the delithiation of the LFP

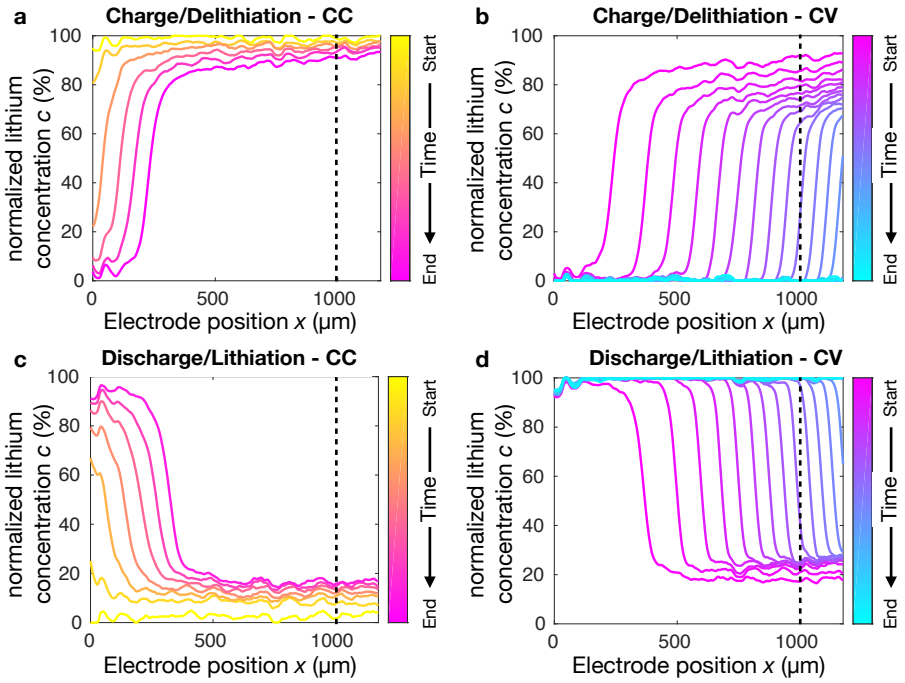

Figure 6: **Charge and discharge concentration profiles** Normalized lithium concentration in the LFP/ATO cathode while charging and discharging in dependency of the electrode position x. (a), (b) Constant current (CC) and constant voltage (CV) for charge process, while (c) and (d) show the same for the discharge process. Each line corresponds to a different time, which is also indicated as color code. Shown time steps are 20 min in the CC modes and 60 min in the CV modes.

particles takes place in the entire electrode, which leads to the observed decreased lithium concentration. Something similar happens during the discharge process shown in figures 6(c) and (d) except for the fact, that the lithiation of LFP particles is restricted by the amount of lithium ions, which are around and which have to move through the entire cathode from the separator/electrode boundary to the inner of the electrode. Hence, for example, if the ion concentration in the electrolyte is low, further lithiation is slowed down and the lithium concentration almost stagnates as seen from the stacked lines in figure 6(d).

3.4. Estimation of apparent diffusion coefficients

In principle, figure 6 provides all information to calculate the apparent diffusion coefficient D in a macroscopical description via Fick's second law in one

dimension,

$$\frac{\partial c}{\partial t} = \frac{\partial}{\partial x}\left(D(c)\frac{\partial c}{\partial x}\right) \quad . \tag{3}$$

Thereby, D gives insights into the dynamics of the investigated cathode in total but lacks detailed information about dynamics in the electrolyte or the particles, itself. Since we're dealing with LFP as a two-phase system, D is explicitly allowed to depend on the concentration of lithium ions c. With the introduction of a new variable $\lambda = x/\sqrt{t}$, which relates space coordinate x and time t, the concentration profiles $c(x)$ of the diffusion process can be described with a scaling analysis [37–39]. Equation 3 is then written as

$$\lambda\frac{\mathrm{d}c}{\mathrm{d}\lambda} = -2\frac{\mathrm{d}}{\mathrm{d}\lambda}\left(D(c)\frac{\mathrm{d}c}{\mathrm{d}\lambda}\right) \quad , \tag{4}$$

which has to account for the boundary conditions $c = C_1 \sim$ constant and $c = C_2 \sim$ constant for $x \ll x_{\mathrm{front}}$ and $x \gg x_{\mathrm{front}}$, respectively. Here, x_{front} is the position of the (de)intercalation front moving with time.

The selected concentration profiles are shown in figures 7(a) and (b). The two phases of the system (α, β) are clearly seen. The evaluation of equation 4 implies a distinct similarity of the solutions, i.e. $c(x,t) = c(\lambda)$, which means that all concentration profiles fall onto a single line due to the introduction of λ. The latter is shown in figures 7(c) and (d) revealing a very good scaling behavior of the concentration profiles. This proves that the observed transport process is diffusion-controlled and an evaluation of D as presented here is justified.

Moreover, this result implies that the presented scheme does not depend on the experimentally applied C-rate for several reasons. First, the estimation of D takes place in the CV mode only. However, different C-rates would cause slightly different reflectivity and lithium concentation profiles since the C-rate has an impact on the length of the CC mode and the spatially-resolved lithium concentration within the electrode would vary at the start of the CV mode. Thus, further lithiation progress in the CV mode is also slightly altered. These effects would be visible as a shift of the reflectivity or normalized lithium concentration lines with respect to the electrode position. In addition, the spacing

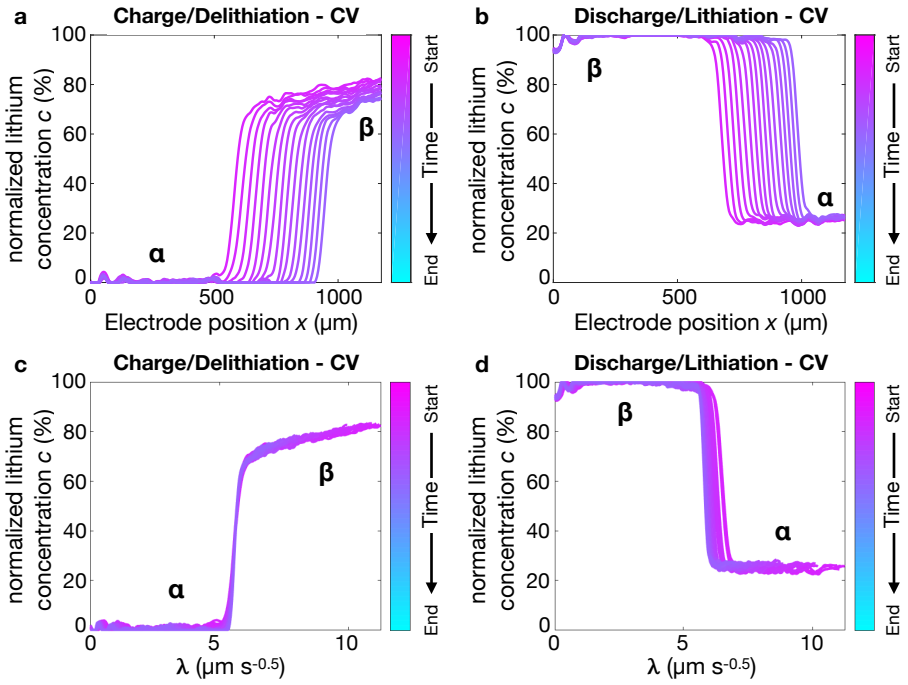

Figure 7: **Scaling analysis of the diffusion process** (a), (b) Normalized lithium concentration profiles in the LFP/ATO cathode shown as colored lines (20 min time steps), which are used for the scaling analysis of the diffusion process as described in the text during the constant voltage (CV) modes for charge and discharge. The two phases of the electrode are marked with α and β. (c), (d) Results of the scaling analysis of the profiles as described in the text.

between those lines would differ as well. Finally, this solely means that certain lithium concentrations within the electrode were reached at different times while different C-rates were applied. Nevertheless, introducing the scaling analysis takes care of those issues almost inherently due to the coupling of space coordinate and time.

A description of the concentration profiles in the presented way has an additional advantage. Since all solutions of equation 4 are similar to each other, it is sufficient to evaluate the diffusion coefficient as

$$D(c) = -\frac{-\int_0^{c(\lambda_{\mathrm{cut}})} \lambda(c')\mathrm{d}c'}{2\,\frac{\mathrm{d}c}{\mathrm{d}\lambda}\big|_{\lambda=\lambda_{\mathrm{cut}}}} \tag{5}$$

from one concentration profile at a single and arbitrarily chosen time [37–39]. Besides the known relations $c(\lambda)$ and $\lambda(c)$, λ_{cut} is determined by the selection

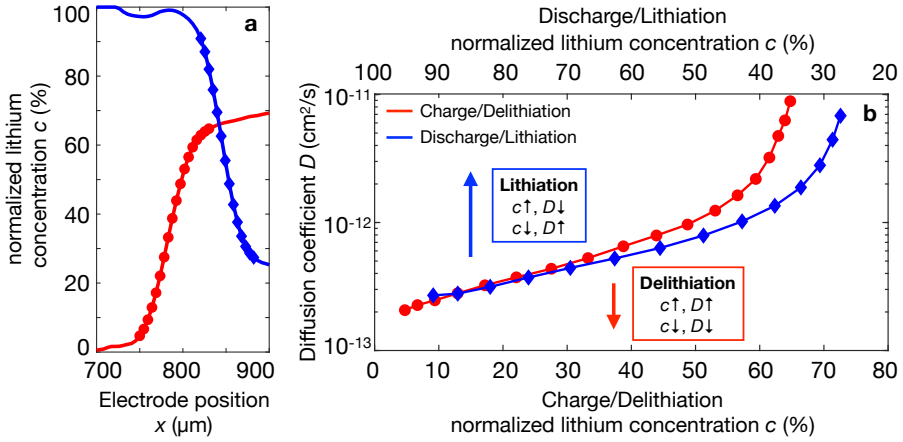

Figure 8: **Concentration profiles and diffusion coefficients** (a) Concentration profiles $c(x)$ at t ∼7 h and t ∼32 h for charging (red) and discharging (blue), which were used for the calculation of the diffusion coefficient D. Colors and markers are also related to (b). (b) Diffusion coefficient D as a function of the normalized lithium concentration c for the charge (delithiation) and discharge (lithiation) process (red and blue markers, respectively). The lines are drawn to guide the eyes.

of c.

The as-calculated diffusion coefficients are shown in figure 8. Markers on the selected concentration profiles upon lithiation (red) and delithiation (blue) in figure 8(a) highlight the lithium concentrations at which D is calculated. Resulting values for D at those concentrations are given in figure 8(b). It is found, that upon lithiation D decreases with increasing c (blue curve, upper x-axis), which might be explained in the following way. If the lithium concentration in the cathode is small, the remaining volume, which can be lithiated is large and the lithiation process is fast. With increasing lithium concentration, this volume is reduced leading to an overall reduction of lithiation as well. The latter would then result in an decreased diffusion coefficient as it is obtained.

Solid-state diffusion coefficients found in the literature vary over a wide range of magnitudes from $10^{-7}\,\mathrm{cm^2\ s^{-1}}$ to $10^{-15}\,\mathrm{cm^2\ s^{-1}}$ [40, 41] depending on theoretical calculations and modeling, experiments on single crystals or investigation of full electrodes. Thereby, state-of-charge, particle size and coating as well as fabrication processes play a crucial role for the reported values. Apart from that,

these diffusion coefficients are directly related to lithium iron phosphate as active material being one part of the entire cathode. Thus, our estimated apparent diffusion coefficients, within the range from $10^{-13}\,\mathrm{cm}^2\ \mathrm{s}^{-1}$ to $10^{-12}\,\mathrm{cm}^2\ \mathrm{s}^{-1}$, are in agreement with commonly accepted values.

A qualitative comparison of the diffusion coefficients of the three cathodes (LFP/ATO, LFP/ITO and LFP/C), which is shown in the Supplemental Material reveal an overall similar behavior. Nevertheless, a comprehensive conclusion is difficult due to the nature of D being an apparent quantity. Each of the cathodes has its own specific properties like porosity, tortuosity, film thickness, etc., which affects the ion dynamics upon cycling. Therefore, a quantitative discussion is solely useful if all electrode parameters are known. Discussing the influences from the additives ATO, ITO and carbon in details is not meaningful for the same reason. However, if cathodes are well characterized, further discussions are possible.

4. Conclusions

We presented a quantitative method to obtain lithium ion dynamics in lithium iron phosphate based cathodes. The method is based on a video microscopy setup and allows for a clear in situ identification of the intercalation and deintercalation of ions in terms of a moving wavefront, i.e. (de)intercalation front, upon battery cycling. Based on this observation, an apparent diffusion coefficient of the entire electrode was obtained within a macroscopic description using Fick's second law of diffusion. By applying a scaling analysis, we mathematically proved that the (de)lithiation process is diffusion controlled in our setup (figures 7(c) and (d)). The apparent diffusion coefficient is the result from a combination of ion migration and diffusion in the liquid electrolyte as well as from the electrochemical (dis)charge reaction at the LFP particles.

We utilized the transparent conducting oxides antimony tin oxide (ATO) and indium tin oxide (ITO) as additives for lithium ion battery cathodes. Both act as electrochomic marker, which significantly enhances the observability of the usually black and non-reflective positive electrodes. Thereby, ATO is presented

for the first time within the field of battery research. A common LFP cathode with carbon additive was investigated as well.

For the future, we think that our presented method is a straightforward adaptable procedure for the characterization of battery cathodes. The implementation of the scaling analysis seems to be very attractive for such types of measurements since it directly determines whether the transport process is diffusion controlled or not. In this sense, this type of analysis could be probably adapted to investigate graphite anodes as well. For those electrodes, the question whether diffusion coefficients can be obtained from Fick's law of diffusion or not is still a hot topic due to the complex ion intercalation in graphite [25–27, 42].

Even though the method does not give detailed microscopical insights, the possibility to observe the electrode directly while evaluating a macroscopical quantity, which characterizes the electrode and describes the motion of lithium ions in situ is beneficial. Hence, a combination with standard in situ techniques and characterization methods is recommended to have more insight into the physical/chemical behavior of the battery electrodes. Additionally, the method itself is not limited to LFP and can be used to investigate a vast variety of cathodes based on lithium nickel manganese cobalt oxide (NMC), lithium cobalt oxide (LCO) or lithium manganese oxide (LMO), for instance. Thereby, the transparent conducting oxides such as antimony tin oxide and indium tin oxide might be used instead of carbon to significantly enhance the observability of the usually black and non-reflective positive electrodes.

Acknowledgments

The work was supported by the German Ministry for Economic Affairs and Energy (BMWi) within the project 'IMBAT' (grant ZF4019009RE7). We want to thank Michael Hahn and Matthias Hahn for offering their chemical lab and their expertise to prepare battery electrodes at EL-Cell GmbH in Hamburg.

References

[1] J. S. Newman, C. W. Tobias, Theoretical analysis of current distribution in porous electrodes, Journal of The Electrochemical Society 109 (12) (1962) 1183–1191.

[2] J. S. Newman, W. Tiedemann, Porous-electrode theory with battery applications, AIChE Journal 21 (1) (1975) 25–41.

[3] M. Doyle, T. F. Fuller, J. S. Newman, Modeling of galvanostatic charge and discharge of the lithium/polymer/insertion cell, Journal of the Electrochemical society 140 (6) (1993) 1526–1533.

[4] M. Doyle, J. S. Newman, The use of mathematical modeling in the design of lithium/polymer battery systems, Electrochimica Acta 40 (13-14) (1995) 2191–2196.

[5] V. Srinivasan, J. S. Newman, Discharge model for the lithium iron-phosphate electrode, Journal of the Electrochemical Society 151 (10) (2004) A1517–A1529.

[6] D. Danilov, P. H. L. Notten, Mathematical modelling of ionic transport in the electrolyte of Li-ion batteries, Electrochimica Acta 53 (17) (2008) 5569–5578.

[7] V. Zadin, D. Danilov, D. Brandell, P. H. L. Notten, A. Aabloo, Finite element simulations of 3D ionic transportation properties in Li-ion electrolytes, Electrochimica Acta 65 (2012) 165–173.

[8] S. Wang, L. Lu, X. Liu, A simulation on safety of LiFePO4/C cell using electrochemical–thermal coupling model, Journal of Power Sources 244 (2013) 101–108.

[9] D. Li, D. L. Danilov, B. Zwikirsch, M. Fichtner, Y. Yang, R.-A. Eichel, P. H. L. Notten, Modeling the degradation mechanisms of C6/LiFePO4 batteries, Journal of Power Sources 375 (2018) 106–117.

[10] N. Yao, L. Heredy, R. Saunders, Emf measurements of electrochemically prepared lithium-aluminum alloy, Journal of The Electrochemical Society 118 (7) (1971) 1039.

[11] W. Weppner, Determination of the kinetic parameters of mixed-conducting electrodes and application to the system li[sub 3]sb, Journal of The Electrochemical Society 124 (10) (1977) 1569.

[12] C. J. Wen, Thermodynamic and mass transport properties of "LiAl", Journal of The Electrochemical Society 126 (12) (1979) 2258.

[13] P. J. Bouwman, B. A. Boukamp, H. J. M. Bouwmeester, P. H. L. Notten, Influence of diffusion plane orientation on electrochemical properties of thin film LiCoO[sub 2] electrodes, Journal of The Electrochemical Society 149 (6) (2002) A699.

[14] H. Xia, L. Lu, G. Ceder, Li diffusion in licoo2 thin films prepared by pulsed laser deposition, Journal of Power Sources 159 (2) (2006) 1422 – 1427.

[15] A. Verma, K. Smith, S. Santhanagopalan, D. Abraham, K. P. Yao, P. P. Mukherjee, Galvanostatic intermittent titration and performance based analysis of LiNi0.5co0.2mn0.3o2cathode, Journal of The Electrochemical Society 164 (13) (2017) A3380–A3392.

[16] S. Alvin, H. S. Cahyadi, J. Hwang, W. Chang, S. K. Kwak, J. Kim, Revealing the intercalation mechanisms of lithium, sodium, and potassium in hard carbon, Advanced Energy Materials 10 (20) (2020) 2000283.

[17] C. G. Hawkins, A. Verma, W. Horbinski, R. Weeks, P. P. Mukherjee, L. Whittaker-Brooks, Decreasing the ion diffusion pathways for the intercalation of multivalent cations into one-dimensional tis2 nanobelt arrays, ACS Applied Materials & Interfaces 12 (19) (2020) 21788–21798.

[18] O. Capron, R. Gopalakrishnan, J. Jaguemont, P. Van Den Bossche, N. Omar, J. Van Mierlo, On the ageing of high energy lithium-ion batter-

ies—comprehensive electrochemical diffusivity studies of harvested nickel manganese cobalt electrodes, Materials 11 (2) (2018) 176.

[19] C.-H. Chen, F. B. Planella, K. O'Regan, D. Gastol, W. D. Widanage, E. Kendrick, Development of experimental techniques for parameterization of multi-scale lithium-ion battery models, Journal of The Electrochemical Society 167 (8) (2020) 080534.

[20] K. Dokko, M. Mohamedi, Y. Fujita, T. Itoh, M. Nishizawa, M. Umeda, I. Uchida, Kinetic characterization of single particles of licoo2 by ac impedance and potential step methods, Journal of the Electrochemical Society 148 (5) (2001) A422.

[21] S. Tang, M. Lai, L. Lu, Li-ion diffusion in highly (0 0 3) oriented licoo2 thin film cathode prepared by pulsed laser deposition, Journal of Alloys and Compounds 449 (1-2) (2008) 300–303.

[22] H. Mehrer, Diffusion in solids: fundamentals, methods, materials, diffusion-controlled processes, Vol. 155, Springer Science & Business Media, 2007.

[23] X. Zhang, T. W. Verhallen, F. Labohm, M. Wagemaker, Direct observation of li-ion transport in electrodes under nonequilibrium conditions using neutron depth profiling, Advanced Energy Materials 5 (15) (2015) 1500498.

[24] C. Chen, J. F. M. Oudenhoven, D. L. Danilov, E. Vezhlev, L. Gao, N. Li, F. M. Mulder, R.-A. Eichel, P. H. L. Notten, Origin of degradation in si-based all-solid-state li-ion microbatteries, Advanced Energy Materials 8 (30) (2018) 1801430.

[25] S. J. Harris, A. Timmons, D. R. Baker, C. Monroe, Direct in situ measurements of Li transport in Li-ion battery negative electrodes, Chemical Physics Letters 485 (4) (2010) 265–274.

[26] P. Maire, H. Kaiser, W. Scheifele, P. Novák, Colorimetric determination of lithium-ion mobility in graphite composite electrodes, Journal of Electroanalytical Chemistry 644 (2) (2010) 127–131.

[27] J. J. Lodico, C.-H. Lai, M. Woodall, H. L. Chan, E. Garcia, W. A. Hubbard, B. Dunn, B. Regan, Irreversibility at macromolecular scales in the flake graphite of the lithium-ion battery anode, Journal of Power Sources 436 (2019) 226841.

[28] V. Roscher, M. Schneider, P. Durdaut, N. Sassano, S. Pereguda, E. Mense, K.-R. Riemschneider, In-situ Electrode Observation as an Optical Sensing Method for Battery State of Charge, IEEE Sensors Application Symposium Glassboro 2017.

[29] V. Roscher, K.-R. Riemschneider, Method and Measurement Setup for Battery State Determination Using Optical Effects in the Electrode Material, IEEE Transactions on Instrumentation and Measurement 2018.

[30] V. Roscher, F. Rittweger, K.-R. Riemschneider, Electrochromic Effect of Indium Tin Oxide in Lithium Iron Phosphate Battery Cathodes for State-of-Charge Determination, ACS Applied Materials & Interfaces 11 (7) (2019) 6900–6906.

[31] A. S. Andersson, J. O. Thomas, The source of first-cycle capacity loss in LiFePO4, Journal of Power Sources 97-98 (2001) 498 – 502.

[32] A. Yamada, H. Koizumi, N. Sonoyama, R. Kanno, Phase change in LixFePO4, Electrochemical and Solid-State Letters 8 (8) (2005) A409–A413.

[33] C. Delmas, M. Maccario, L. Croguennec, F. L. Cras, F. Weill, Lithium deintercalation in LiFePO4 nanoparticles via a domino-cascade model, Nature Materials 7 (2008) 665–671.

[34] G. Brunetti, D. Robert, P. Bayle-Guillemaud, J. L. Rouvière, E. F. Rauch, J. F. Martin, J. F. Colin, F. Bertin, C. Cayron, Confirmation of the Domino-Cascade Model by LiFePO4/FePO4 Precession Electron Diffraction, Chemistry of Materials 23 (20) (2011) 4515–4524.

[35] X. Zhang, M. van Hulzen, D. P. Singh, A. Brownrigg, J. P. Wright, N. H. van Dijk, M. Wagemaker, Rate-Induced Solubility and Suppression of the First-Order Phase Transition in Olivine LiFePO4, Nano Letters 14 (5) (2014) 2279–2285.

[36] X. Zhang, M. Van Hulzen, D. P. Singh, A. Brownrigg, J. P. Wright, N. H. Van Dijk, M. Wagemaker, Direct view on the phase evolution in individual LiFePO4 nanoparticles during Li-ion battery cycling, Nature communications 6 (2015) 8333.

[37] L. Boltzmann, Zur Integration der Diffusionsgleichung bei variabeln Diffusionscoefficienten, Annalen der Physik 289 (13) (1894) 959–964.

[38] J. Crank, et al., The mathematics of diffusion, Oxford university press, 1979.

[39] F. Den Broeder, S. Van der Molen, M. Kremers, J. Huiberts, D. Nagengast, A. Van Gogh, W. Huisman, N. Koeman, B. Dam, J. Rector, et al., Visualization of hydrogen migration in solids using switchable mirrors, Nature 394 (6694) (1998) 656.

[40] R. Malik, D. Burch, M. Bazant, G. Ceder, Particle Size Dependence of the Ionic Diffusivity, Nano Letters 10 (10) (2010) 4123–4127.

[41] G. K. P. Dathar, D. Sheppard, K. J. Stevenson, G. Henkelman, Calculations of Li-Ion Diffusion in Olivine Phosphates, Chemistry of Materials 23 (17) (2011) 4032–4037.

[42] M. Heß, P. Novák, Shrinking annuli mechanism and stage-dependent rate capability of thin-layer graphite electrodes for lithium-ion batteries, Electrochimica Acta 106 (2013) 149 – 158.